





Article

Optical Characteristics of ZnCuInS/ZnS (Core/Shell) Nanocrystal Flexible Films Under X-Ray Excitation

George Saatsakis ¹, Nektarios Kalyvas ², Christos Michail ², Konstantinos Ninos ³, Athanasios Bakas ³, Christina Fountzoula ³, Ioannis Sianoudis ³, George E. Karpetas ⁴, George Fountos ², Ioannis Kandarakis ², Ioannis Valais ² and George Panayiotakis ^{1,*}

¹ Department of Medical Physics, Faculty of Medicine, University of Patras, GR-15310 Rion, Greece

² Department of Biomedical Engineering, Radiation Physics, Materials Technology, and Biomedical Imaging Laboratory, University of West Attica, 122 10 Athens, Greece

³ Department of Biomedical Sciences, University of West Attica, 122 10 Athens, Greece

⁴ Department of Medical Physics, Faculty of Medicine, University of Thessaly, 41110 Larissa, Greece

* Correspondence: panayiot@upatras.gr

Received: 6 June 2019; Accepted: 3 July 2019; Published: 4 July 2019



Abstract: The aim of this article is to evaluate optical characteristics, such as the intrinsic conversion efficiency and the inherent light propagation efficiency of three polymethyl methacrylate (PMMA)/methyl methacrylate (MMA) composite ZnCuInS/ZnS (core/shell) nanocrystal flexible films. The concentrations of these were 100 mg/mL, 150 mg/mL, and 250 mg/mL, respectively. Composite films were prepared by homogeneously diluting dry powder quantum dot (QD) samples in toluene and subsequently mixing these with a PMMA/MMA polymer solution. The absolute luminescence efficiency (*AE*) of the films was measured using X-ray excitation. A theoretical model describing the optical photon propagation in scintillator materials was used to calculate the fraction of the generated optical photons passed through the different material layers. Finally, the intrinsic conversion efficiency was calculated by considering the QD quantum yield and the optical photon emission spectrum.

Keywords: quantum dots; nanocrystals; ZnCuInS/ZnS; PMMA; luminescence efficiency

1. Introduction

In recent years nanophosphors [1–4] and quantum dots (QDs) [5,6] have been investigated as possible sensors for many applications, including but not limited to, medicine, displays, and solar energy harvesting. QDs are semiconductor nanocrystals, in which optical properties are controlled by their particle size, which is in the nanoscale range, as well as shape and composition [7,8]. QDs have attracted attention since their emission spectra and electronic properties have found application as biological labels, light emitting devices, and optoelectronic sensors [9–11]. In addition, QDs and other scintillating materials have been proposed as candidates for ionizing radiation detectors [12–15]. On the other hand, increased awareness of the harmful effects of toxic heavy-metal compounds that could be used in QDs has led authorities to provide relevant legislation. The European Union Directive 2011/65/EU "Restriction of the Use of Certain Hazardous Substances" (RoHS) limits the amount of cadmium, lead, and mercury that can be used in electrical and electronic equipment to protect the consumer and the environment from the effects of heavy-metal toxicity. Our group has reported initial experimental results, regarding the response of QDs employing Zn, S, and Cd in their synthesis, as a candidate for radiation detection. The detectors consisted of QDs infused in a polymethyl methacrylate (PMMA)/methyl methacrylate (MMA) toluene [12,16–18]. However, the use of cadmium, a proven carcinogen with (LD₅₀) toxicity, of 100–300 mg/kg [19] is restricted ten-fold. Where LD stands for "Lethal Dose". LD₅₀ is the amount of a material, given all at once, which causes the death of 50% (one

half) of a group of test animals. Therefore, it is of importance to examine a cadmium-free QD and assess its performance as a radiation detector. ZnCuInS/ZnS QDs are cadmium-free, hydrophobic core-shell structured nanocrystals with an inner core of zinc copper indium sulfide encapsulated by an outer core of zinc sulfide [20–24]. In this study, ZnCuInS/ZnS QDs infused in a PMMA/MMA toluene substrate were excited by X-rays and their X-ray luminescence efficiency, also known as absolute efficiency (*AE*), was experimentally determined. The optical photon transmission properties of the ZnCuInS/ZnS were determined theoretically. To our knowledge, this is the first time the Absolute Efficiency of ZnCuInS/ZnS QDs infused in a PMMA/MMA substrate have been theoretically examined and their optical transmission properties investigated. The current work is the first step towards a thorough investigation regarding the estimation of optimum QD-nanocrystal-based detector performance for various combinations of thin film preparation methods, scintillator concentration, and X-ray energy. This will allow the optimization of QDs synthesis and PMMA/MMA substrate infusion process.

2. Materials and Methods

PMMA and MMA were purchased from Sigma Aldrich and Alfa Aesar GmbH, respectively, with the purity of the ingredients reaching 99%. Toluene was purchased from Fluka Chemica with a purity of more than 99%. ZnCuInS/ZnS QDs were purchased from PlasmaChem GmbH in powder form with 5 nm particle size and a 530 nm ± 15 nm emitting wavelength. ZnCuInS/ZnS quantum dots were selected due to their emission spectrum, which is compatible with the most common digital optical sensors [25,26]. In addition, ZnCuInS/ZnS does not contain any high toxicity compounds like cadmium, lead, mercury, or arsenide, making it an attractive alternative for use in several applications. For the QD/PMMA fabrication, a PMMA/MMA low viscosity solution was prepared by mixing PMMA powder with liquid MMA [15,24]. Three samples of ZnCuInS/ZnS QDs in toluene were prepared by dissolving 100 mg, 150 mg, and 250 mg in 1 mL toluene in order to achieve concentrations of 100 mg/mL, 150 mg/mL, and 250 mg/mL, respectively. Finally, 1.5 mL of the PMMA/MMA solution was added to each sample, with samples stirred in a vortex to fabricate the final solution. Final samples were poured into molds to obtain a cylindrical shaped scintillator of 1.9 cm base diameter and 0.9 mm height in the form of a thin film. The molds were placed under vacuum conditions to remove any entrapped air bubbles and in a drying chamber under 50 °C to eliminate residual solvent. A more detailed description regarding the QD/PMMA scintillator fabrication can be found in the literature [12,16,17].

The QD/PMMA films were irradiated utilizing a BMI General Medical Merate X-ray tube (General Medical Merate S.P.A., Bergamo, Italy) with a W anode and filtration equivalent to 2 mm Al, with tube voltages ranging from 50 to 130 kVp. An additional 20 mm filtration was introduced in the beam to simulate beam quality attenuation by a human body [17,27–31]. The thin films were positioned in an integration sphere (Oriel 70451) and their light output was measured by means of a calibrated photomultiplier in connection with a Keithley Model 6430 Sub-Femtoamp Remote SourceMeter (Keithley Instruments Inc., Cleveland, OH, USA) electric current meter. The experimental setup is shown in Figure 1. The exposure rate (\dot{X}) of the X-rays incident on the film was measured with an RTI PIRANHA multimeter. The absolute luminescence efficiency was calculated as a ratio of the light energy flux, Ψ_λ , emitted by the scintillator over the incident exposure rate [1,25,27–30], that is:

$$AE = \frac{\Psi_\lambda}{\dot{X}} \quad (1)$$

The considered theoretical model has already been applied for scintillators with a crystal-like powder and structured form [32–35]. In this model, the transfer of the signal in the scintillator can be modeled by accounting for the transmission per layer. A fraction of the incident X-ray energy is assumed to be absorbed in each layer. Optical photons are generated and assumed to propagate either in a forward or backward direction. The optical photon flux is reduced either by internal optical photon absorption or by optical photon escape when the photons were incident on the surfaces of the crystal [32–34]. It has been assumed that per crystal layer only a fraction, hereafter called *k*, propagates

to the next layer. When the optical photons reached the outer layer of the scintillator, they were either reflected towards the detector or escaped to the output.

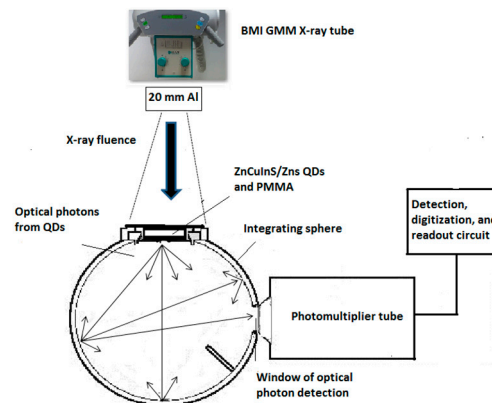


Figure 1. The experimental setup for ZnSCdS/ZnS quantum dot (QD) irradiation. Legend: PMMA, polymethyl methacrylate.

If a scintillator with a thickness T , divided into N elementary layers of thickness $\Delta t = T/N$ is considered, then in each elementary layer, at position n , a fraction of the incident photons deposit their energy, E . By assuming exponential attenuation of the X-ray photons, the number of X-rays absorbed in a layer between t and $t + \Delta t$ is equal to

$$f(E)e^{-\mu n \Delta t} \mu \Delta t \quad (2)$$

where $f(E)$ is the number of the spectrum X-rays of energy E and μ is the X-ray absorption coefficient for energy E [33–35]. The absorbed X-ray energy is transformed into optical photon energy in the scintillator. The number of the produced optical photons in the n th layer L_n can be calculated as

$$L_n(E) = f(E)e^{-\mu n \Delta t} \mu \Delta t n_C \frac{E}{E_\lambda} \quad (3)$$

where n_C is the intrinsic conversion efficiency, defined as the fraction of the irradiation photon energy that is turned into optical photon energy, and E_λ is the optical photon energy [33–36]. The value of n_C , as well as the optical photon emission spectrum, is largely affected by the scintillator synthesis method [22,35,37–42].

The value of n_C for the ZnCuInS/ZnS QDs was calculated according to literature data, where a quantum yield (QY) of 33.65% [21] has been reported for approximately 350 nm excitation and optical photon production at approximately 530 nm as

$$n_C = \frac{QY(hc/\lambda_{prod.})}{100(hc/\lambda_{excit.})} \quad (4)$$

where λ is the photon wavelength.

It is assumed that half of the produced optical photons are propagating forward and half backward. By accounting for all the reflections between the scintillator input and output interfaces, the fraction of the optical photons that escape the output equals to [40]

$$M_n = (1 - R) \left[\frac{k^{N-n}}{1 - k^{2N}R^2} + Rk^{n+N} \frac{k^{2N}R^2}{1 - k^{2N}R^2} \right] \quad (5)$$

If all the layers are considered, the total number of optical photons produced by X-rays of energy E that escape to the output equals to [33,34]

$$M(E) = \sum_{n=1}^N f(E) e^{-\mu n \Delta t} \mu \Delta t n c \frac{E}{E_\lambda} (1-R) \left[\frac{k^{N-n}}{1-k^{2N}R^2} + Rk^{n+N} \frac{k^{2N}R^2}{1-k^{2N}R^2} \right] \quad (6)$$

For the entire X-ray energy spectrum, AE can be calculated as

$$AE = \frac{\sum_{E=E_{\min}}^{E_{\max}} \gamma(E)M(E)}{\sum_{E=E_{\min}}^{E_{\max}} f(E)} \quad (7)$$

where $\gamma(E)$ is a conversion factor converting energy fluence (W/m^2) into exposure rate (mR/s), E_{\min} is the lowest non-zero spectral component energy of the X-ray spectrum, and E_{\max} corresponds to the maximum energy component of the X-ray spectrum. The total reflection, R , in Equations (3) and (4) has been calculated as

$$R = \frac{(n-1)^2}{(n+1)^2} \quad (8)$$

where n is the diffraction coefficient of PMMA at 535 nm taken as equal to 1.4935 [43]. The attenuation coefficients of ZnCuInS/ZnS were calculated by Xmutat [44] by considering 0.04 mol Cu, 0.2 mol Zn, 0.2 mol In, and 0.2 mol S in the mixture for ZnCuInS/ZnS production [21], leading to fractional weights of 5.7%, 28.9%, 51.1%, and 14.2%, respectively. In the above reference the emission spectrum of the ZnCuInS/ZnS QDs as well as their size were very close to those used in this study, that is, the above reference had a wavelength of 530 nm and size of 4–5 nm [45]. The value of k used in Equations (5) to (7) was determined by fitting Equation (7) to the experimental AE results.

3. Results

The intrinsic conversion efficiency was found to be equal to 0.22. This value is higher than other values reported for non-QD scintillators [1,35,36]. The physical properties of ZnCuInS/ZnS related to ionizing radiation interaction probability, as calculated by Xmutat [44], were 2.7×10^{23} electrons/g, $Z_{\text{eff}} = 41.18$, and material density $5.34 \text{ g}/\text{cm}^3$.

In Figure 2, the energy absorption coefficients of ZnCuInS/ZnS for energies in the range of 10 keV to 130 keV are demonstrated. The K-shell energy peak, corresponding to the enhanced photoelectric absorption, is observed at approximately 28 keV. The inset in Figure 2 shows the normalized luminescence spectrum of the examined QDs [46].

The optical emission characteristics of the QDs/PMMA thin films depends also upon the core-shell structure of the QDs. It has been reported [21], that although the wide-angle XRD patterns of ZnCuInS QDs show peaks of a tetragonal chalcopyrite structure, when coated with a ZnS shell, the QDs maintain a tetragonal structure. However, the diffraction peaks shift to larger angles, indicating a further alloying, since ZnS has a smaller lattice constant compared to Cu-In-S [21].

In Figure 3, the values of parameter k , as presented in Equation (3), show the optical photon transmission per layers of thickness $5 \mu\text{m}$. The values were calculated between 0.700–0.717 (average 0.708), 0.681–0.701 (average 0.691), and 0.638–0.648 (average 0.643) for 100 mg/mL, 150 mg/mL, and 250 mg/mL QDs, respectively. It may be observed that the optical photon transmission per layer decreased when the QD concentration is increased. Corresponding k values for single crystal scintillators are $k > 0.99$ for $\text{Gd}_2\text{SiO}_5:\text{Ce}$, $\text{Lu}_2\text{SiO}_5:\text{Ce}$ and $\text{YAlO}_3:\text{Ce}$ [33], $k = 0.97$ for CsI:Tl columnar phosphors [34] and $0.38 < k < 0.7$ for $\text{Cd}_2\text{O}_2\text{S}:\text{Pr}$ granular phosphor [35].

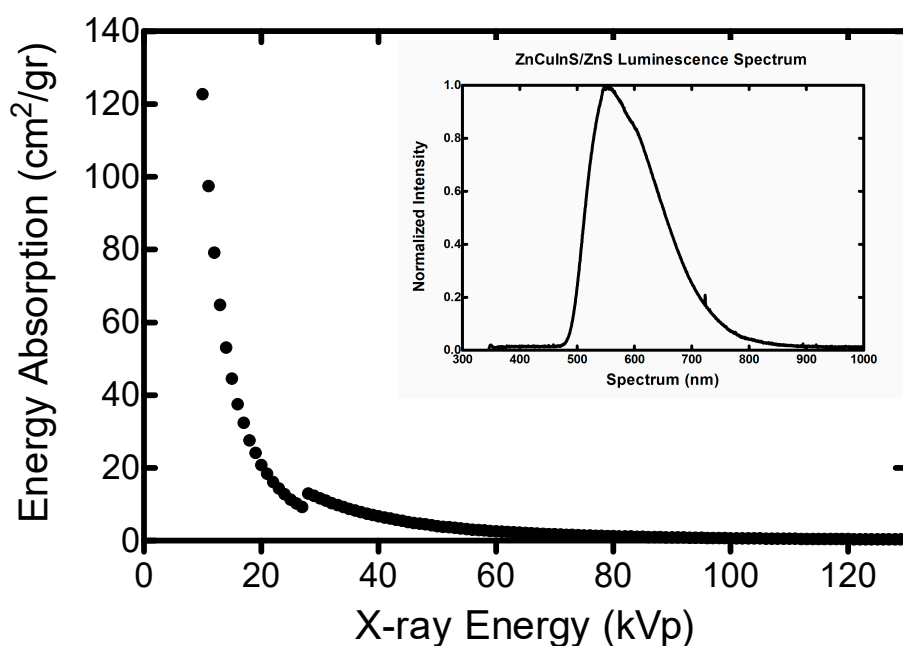


Figure 2. The mass energy absorption coefficient of ZnCuInS/ZnS QDs. The inset shows the QDs' luminescence spectrum.

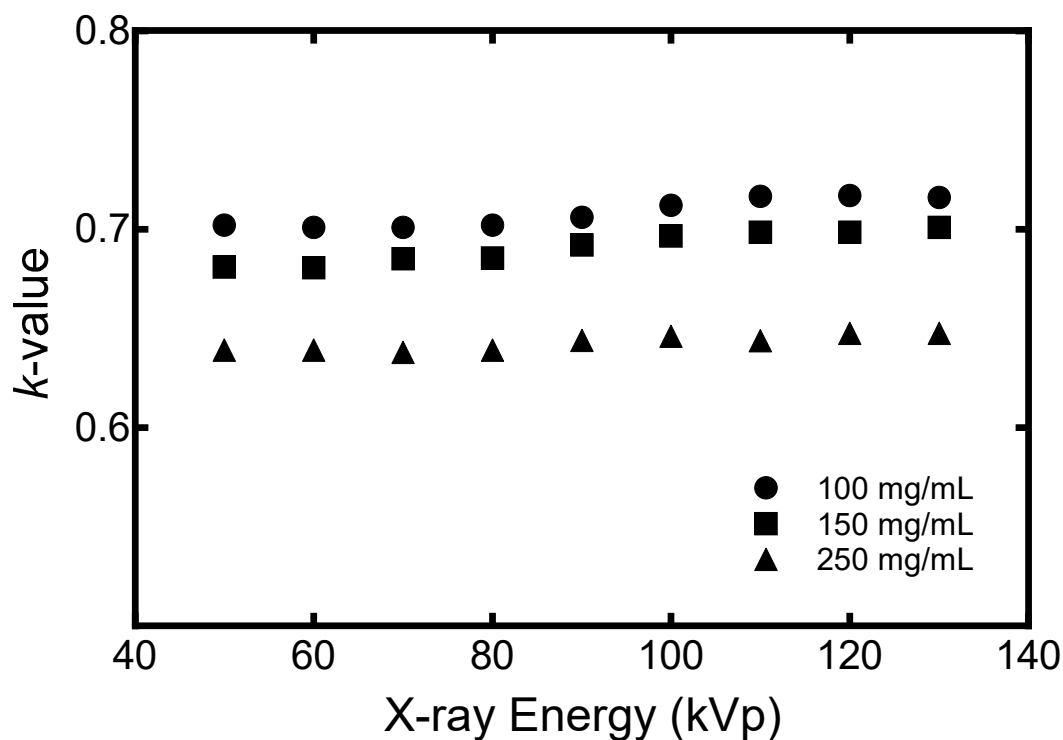


Figure 3. The optical photon transmission per 5 μm (k value) for the 100 mg/mL, 150 mg/mL, and 250 mg/mL ZnCuInS/ZnS concentrations.

In addition, in Figure 4, a comparison between the experimental AE values and the theoretical predicted average k values of $k = 0.708$, $k = 0.691$, and $k = 0.643$ for 100 mg/mL, 150 mg/mL, and 250 mg/mL QDs, respectively is shown. The deviation between the theoretical and experimental AE results for the average k values was between 0.5% and 9.1%. The theoretical model showed better performance with the thin film of 250 mg/mL. The corresponding experimental error was within 5%.

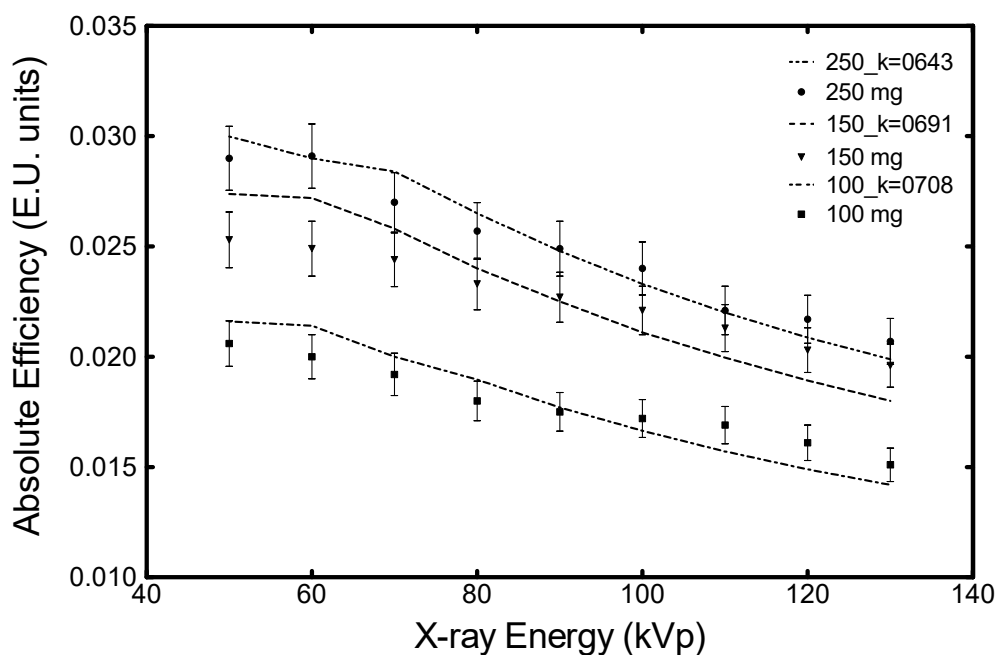


Figure 4. Comparison between experimental and theoretical (based on Equation (5)) absolute efficiency (AE) results in E.U. (1 E.U. = $1 \mu\text{W m}^{-2}/\text{mR s}^{-1}$).

In Figure 5 the change in transmission per $5 \mu\text{m}$ layer with respect to the ZnCuInS/ZnS concentration is shown. By fitting these results, the following empirical formula was able to be obtained:

$$k = (-0.0004 \cdot C) + 0.7549 \tag{9}$$

In this equation, C is the QD concentration in mg/mL.

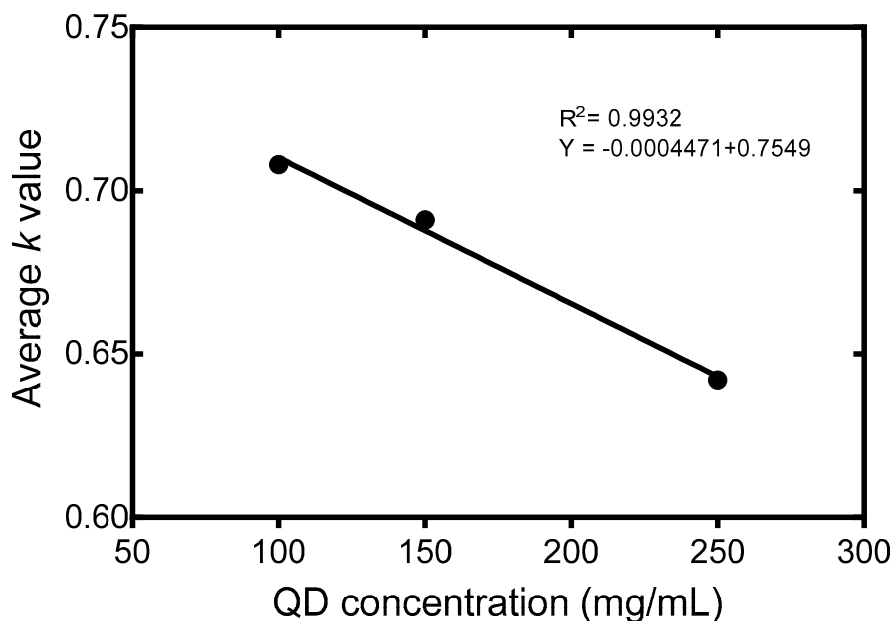


Figure 5. Effect of ZnCuInS/ZnS concentration on the k value.

By observing the experimental AE results, it can be deduced that AE increases with ZnCuInS/ZnS concentration. To further investigate the AE change with increasing QD concentration, theoretical AE values for 300 mg/mL, 400 mg/mL, and 450 mg/mL were calculated and are presented in Figure 6.

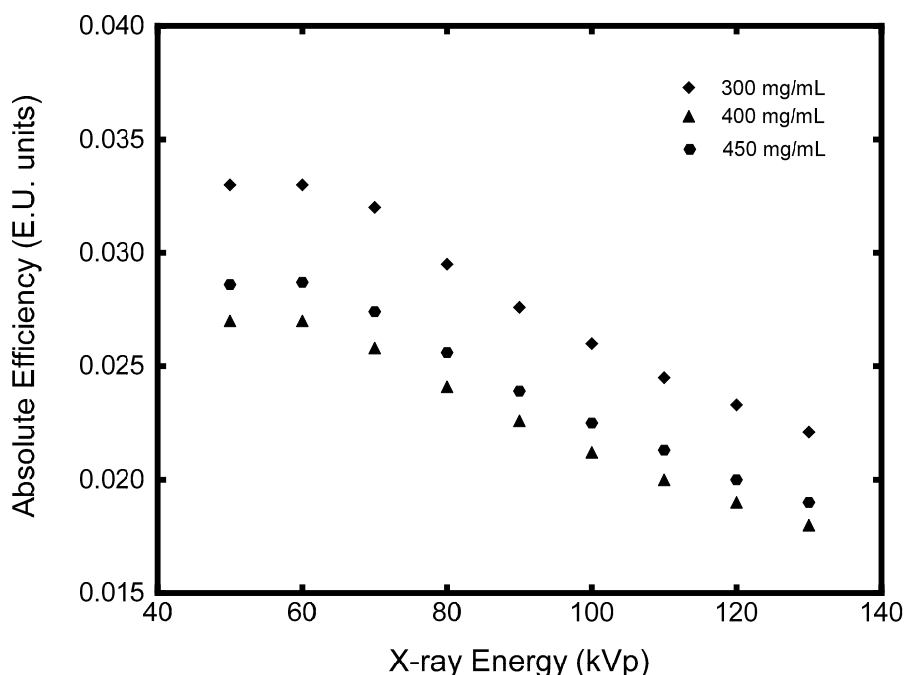


Figure 6. Comparison between predicted AE values for 300 mg/mL, 400 mg/mL, and 450 mg/mL ZnCuInS/ZnS concentrations for X-ray tube voltages used for radiographic applications.

The *k* values for 300 mg/mL, 400 mg/mL, and 450 mg/mL which were calculated by Equation (9) were 0.6349, 0.5949, and 0.5749 respectively. By considering that the K-edge of ZnCuInS/ZnS is approximately 28 keV, the possible utility of our QDs in lower X-ray energy applications was investigated by calculating the corresponding AE values for monoenergetic photons with energies of 10 keV, 15 keV, and 28 keV. The results are shown in Figure 7. It can be demonstrated that AE at 28 keV, just above the QD K-edge, as shown in Figure 2, produces the highest AE value.

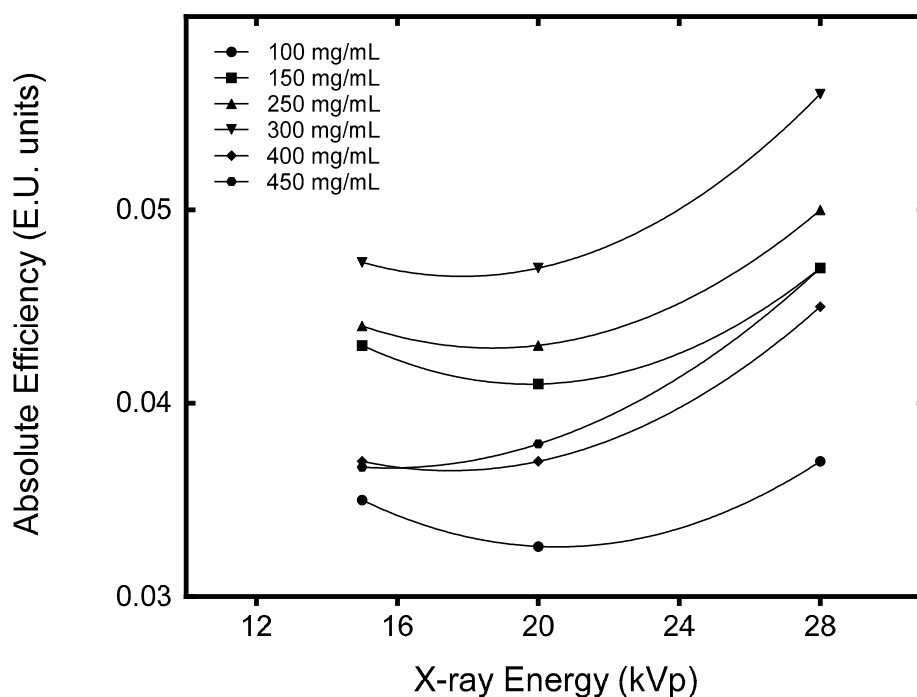


Figure 7. Predicted AE values for 100 mg/mL, 150 mg/mL, 250 mg/mL, 300 mg/mL, 400 mg/mL, and 450 mg/mL at X-ray energies of 15 keV, 20 keV, and 28 keV.

4. Discussion

As shown in Figure 3, a higher QD concentration leads to a lower optical photon transmission in the detector, since the increased QD material increases the optical photon absorption and scattering sites within the thin film. Thus, the light generated suffers more losses while propagating to the output. This trend, however, is not demonstrated straightforwardly by our experimental *AE* data shown in Figure 4, where the higher the QD concentration the better the *AE*. The shape of the *AE* curve can be justified by the fact that the higher QD concentration offers more sites for X-ray energy absorption and optical photon generation. Thus, for the 250 mg/mL thin film, the number of optical photons generated per layer in the scintillator, that is, the sum

$$\sum_E \sum_n L_n(E) \quad (10)$$

increases with QD concentration. The overall performance of the ZnCuInS/ZnS QDs, with respect to *AE*, is a combination of the number of the optical photons generated and the rate of their absorption as they propagate within the scintillator mass. It was found that absolute efficiency increases with QD concentration. However, it seems to saturate over a 400 mg/mL QD concentration, as shown by Figure 6, where the corresponding *AE* values of 400 mg/mL and 450 mg/mL films are very close. Even though the higher concentration increases the probability of X-ray absorption in ZnCuInS/ZnS mass and the production of optical photons, the overall attenuation of light as it propagates to the output is also increased. The latter is demonstrated by the effect on the predicted *k* value with increasing concentration. For example, the transmission of the optical photons per layer for the 450 mg/mL concentration is 9.5%, which is less than the 300 mg/mL concentration. For the X-ray tube voltages used in diagnostic radiology applications, the optimum performance was found for the 300 mg/mL concentration in all tube voltages. The calculated *AE* values, however, were found to be below other values reported in the literature for non-QD powder phosphors [1,25,27–30]. Results indicate that the nanocrystals used in our experiments may be more promising in modalities using X-ray energies below 28 keV, such as XRD or dedicated equipment for small animal imaging and tissue sample characterization. The presented results are based on the optical parameters derived from the experimental *AE* data of the prepared thin films. Further investigation into the improvement of the QD thin film preparation procedure and the use of other scintillator concentrations may alter the X-ray absorption properties, as well as the optical transmittance per layer of the detector, and improve its efficiency.

5. Conclusions

In this work, the performance of three compound PMMA/QD nanocrystal films, fabricated in our laboratory, was experimentally and theoretically evaluated under X-ray excitation. It was found that the absolute efficiency increases with ZnCuInS/ZnS concentration but that the gain is negligible for concentrations above 400 mg/mL. The intrinsic conversion was calculated as 0.22, while the optical photon attenuation in the material was calculated between 64.3% to 70.8% for QD concentrations between 100 mg/mL to 250 mg/mL, respectively. The theoretical investigation suggested that ZnCuInS/ZnS QDs might be more efficient in instrumentation using lower X-ray energies, such as XRD or dedicated equipment for small animal imaging and tissue sample characterization.

Author Contributions: Conceptualization, G.S., N.K.; methodology, G.S., I.V., N.K., G.P. and I.K.; software, N.K.; validation, N.K. and G.S.; formal analysis, G.S., C.M., N.K., and I.V.; investigation, G.S., C.M., N.K., G.P., K.N., I.S., and I.V.; resources, G.S., K.N., C.F. and A.B.; data curation, G.S., C.M., N.K., G.E.K., I.V. and G.P.; writing—original draft preparation, G.S., N.K. and C.M.; writing—review and editing, G.S., N.K., I.K., and I.V.; visualization, G.S., N.K., and G.F.; supervision, I.K., G.P. and I.V.; project administration, G.S., N.K., K.N., G.F., G.P. and I.V.; funding acquisition, G.S., I.V., and G.P.

Funding: This research was funded by the Institutional Open Access Program (IOAP) of the University of Patras and the University of West Attica.

Conflicts of Interest: The authors declare no conflict of interest.

References

1. Kalyvas, N.; Liaparinos, P.; Michail, C.; David, S.; Fountos, G.; Wójtowicz, M.; Zych, E.; Kandarakis, I. Studying the luminescence efficiency of $\text{Lu}_2\text{O}_3:\text{Eu}$ nanophosphor material for digital X-ray imaging applications. *Appl. Phys. A* **2012**, *106*, 131–136. [CrossRef]
2. Seferis, I.; Michail, C.; Valais, I.; Zeler, J.; Liaparinos, P.; Fountos, G.; Kalyvas, N.; David, S.; Stromatia, F.; Zych, E.; et al. Light emission efficiency and imaging performance of $\text{Lu}_2\text{O}_3:\text{Eu}$ nanophosphor under X-ray radiography conditions: Comparison with $\text{Gd}_2\text{O}_2\text{S}:\text{Eu}$. *J. Lumin.* **2014**, *151*, 229–234. [CrossRef]
3. Lai, C.-F.; Wang, Y.-C. Colloidal Photonic Crystals Containing Silver Nanoparticles with Tunable Structural Colors. *Crystals* **2016**, *6*, 61. [CrossRef]
4. He, Z.; Zhang, C.; Dong, Y.; Wu, S.-T. Emerging Perovskite Nanocrystals-Enhanced Solid-State Lighting and Liquid-Crystal Displays. *Crystals* **2019**, *9*, 59. [CrossRef]
5. Zych, E.; Meijerink, A.; de Mello Doneg, C. Quantum efficiency of europium emission from nanocrystalline powders of $\text{Lu}_2\text{O}_3:\text{Eu}$. *J. Phy. Condens. Matter.* **2003**, *15*, 5145–5155. [CrossRef]
6. Konstantatos, G.; Sargent, E.H. Colloidal quantum dot photodetectors. *Infrared Phys. Technol.* **2011**, *54*, 278–282. [CrossRef]
7. Siffalovic, P.; Badanova, D.; Vojtko, A.; Jergel, M.; Hodas, M.; Pelletta, M.; Sabol, D.; Macha, M.; Majkova, E. Evaluation of low-cadmium ZnCdSeS alloyed quantum dots for remote phosphor solid-state lighting technology. *Appl. Opt.* **2015**, *54*, 7094. [CrossRef]
8. Zeng, R.; Sun, Z.; Cao, S.; Shen, R.; Liu, Z.; Long, J.; Zheng, J.; Shen, Y.; Lin, X. A facile route to aqueous $\text{Ag}:\text{ZnCdS}$ and $\text{Ag}:\text{ZnCdSeS}$ quantum dots: Pure emission color tunable over entire visible spectrum. *J. Alloys. Compd.* **2015**, *632*, 1–9. [CrossRef]
9. Zhang, C.; Du, L.; Liu, C.; Li, Y.; Yang, Z.; Cao, Y.-C. Photostable epoxy polymerized carbon quantum dots luminescent thin films and the performance study. *Results Phy.* **2016**, *6*, 767–771. [CrossRef]
10. Guo, S.; Konopny, L.; Popovitz-Biro, R.; Cohen, H.; Sirota, M.; Lifshitz, E.; Lahav, M. Topotactic Release of CdS and $\text{Cd}_{1-x}\text{Mn}_x\text{S}$ from Solid Thioalkanoates with Ammonia to Yield Quantum Particles Arranged in Layers Within an Organic Composite. *Adv. Mater.* **2000**, *12*, 302–306. [CrossRef]
11. Eychmüller, A. Structure and Photophysics of Semiconductor Nanocrystals. *J. Phy. Chem. B* **2000**, *104*, 6514–6528. [CrossRef]
12. Valais, I.; Michail, C.; Fountzoula, C.; Tseles, D.; Yannakopoulos, P.; Nikolopoulos, D.; Bakas, A.; Fountos, G.; Saatsakis, G.; Sianoudis, I.; et al. On the response of alloyed ZnCdSeS quantum dot films. *Results Phys.* **2017**, *7*, 1734–1736. [CrossRef]
13. Michail, C.; Karpetas, G.; Kalyvas, N.; Valais, I.; Kandarakis, I.; Agavanakis, K.; Panayiotakis, G.; Fountos, G. Information Capacity of Positron Emission Tomography Scanners. *Crystals* **2018**, *8*, 459. [CrossRef]
14. Salomoni, M.; Pots, R.; Auffray, E.; Lecoq, P. Enhancing Light Extraction of Inorganic Scintillators Using Photonic Crystals. *Crystals* **2018**, *8*, 78. [CrossRef]
15. Maddalena, F.; Tjahjana, L.; Xie, A.; Zeng, S.; Wang, H.; Coquet, P.; Drozdowski, W.; Dujardin, C.; Dang, C.; Birowosuto, M.D.; et al. Inorganic, Organic, and Perovskite Halides with Nanotechnology for High-Light Yield X- and γ -ray Scintillators. *Crystals* **2019**, *9*, 88. [CrossRef]
16. Valais, I.; Michail, C.; Fountzoula, C.; Fountos, G.; Saatsakis, G.; Karabotsos, A.; Panayiotakis, G.S.; Kandarakis, I. Polymer Based Thin Film Screen Preparation Technique. *J. Phys. Conf. Ser.* **2017**, *931*, 012035. [CrossRef]
17. Saatsakis, G.; Valais, I.; Michail, C.; Fountzoula, C.; Fountos, G.; Koukou, V.; Martini, N.; Kalyvas, N.; Bakas, A.; Sianoudis, I.; et al. Preliminary Study of $\text{ZnS}:\text{Mn}^{2+}$ Quantum Dots Response Under UV and X-Ray Irradiation. *J. Phys. Conf. Ser.* **2017**, *931*, 012030. [CrossRef]
18. Pang, L.; Shen, Y.; Tetz, K.; Fainman, Y. PMMA quantum dots composites fabricated via use of pre-polymerization. *Opt. Express* **2005**, *13*, 44. [CrossRef]
19. Public Health England, Cadmium: Health Effects, Incident Management And Toxicology Information On Cadmium, For Responding To Chemical Incidents [Online]. Available online: <https://www.gov.uk/government/publications/cadmium-properties-incident-management-and-toxicology> (accessed on 3 July 2019).

20. Dong, X.; Xu, J.; Shi, S.; Zhang, X.; Li, L.; Yin, S. Electroluminescence from ZnCuInS/ZnS quantum dots/poly(9-vinylcarbazole) multilayer films with different thicknesses of quantum dot layer. *J. Phys. Chem. Solids* **2017**, *104*, 133–138. [[CrossRef](#)]
21. Jia, Y.; Wang, H.; Xiang, L.; Liu, X.; Wei, W.; Ma, N.; Sun, D. Tunable emission properties of core-shell ZnCuInS-ZnS quantum dots with enhanced fluorescence intensity. *J. Mater. Sci. Technol.* **2018**, *34*, 942–948. [[CrossRef](#)]
22. Guo, W.; chen, N.; Tu, Y.; Dong, C.; Zhang, B.; Hu, C.; Chang, J. Synthesis of Zn-Cu-In-S/ZnS Core/Shell Quantum Dots with Inhibited Blue-Shift Photoluminescence and Applications for Tumor Targeted Bioimaging. *Theranostics* **2013**, *3*, 99–108. [[CrossRef](#)]
23. Wang, X.; Liang, Z.; Xu, X.; Wang, N.; Fang, J.; Wang, J.; Xu, G. A high efficient photoluminescence Zn-Cu-In-S/ZnS quantum dots with long lifetime. *J. Alloys Compd.* **2015**, *640*, 134–140. [[CrossRef](#)]
24. American Elements, ZnCuInS/ZnS Quantum Dots [Online]. Available online: <https://www.americanelements.com/zncuins-zns-quantum-dots> (accessed on 3 July 2019).
25. Michail, C.M.; Fountos, G.P.; Liaparinos, P.F.; Kalyvas, N.E.; Valais, I.; Kandarakis, I.S.; Panayiotakis, G.S. Light emission efficiency and imaging performance of Gd₂O₂S:Eu powder scintillator under x-ray radiography conditions: Light emission efficiency and imaging performance of Gd₂O₂S:Eu. *Med. Phys.* **2010**, *37*, 3694–3703. [[CrossRef](#)]
26. Magnan, P. Detection of visible photons in CCD and CMOS: A comparative view. *Nucl. Instrum. Methods Phys. Res. A* **2003**, *504*, 199–212. [[CrossRef](#)]
27. Kalivas, N.; Valais, I.; Nikolopoulos, D.; Konstantinidis, A.; Gaitanis, A.; Cavouras, D.; Nomicos, C.D.; Panayiotakis, G.; Kandarakis, I. Light emission efficiency and imaging properties of YAP:Ce granular phosphor screens. *Appl. Phys. A* **2007**, *89*, 443–449. [[CrossRef](#)]
28. Kandarakis, I.; Cavouras, D.; Nikolopoulos, D.; Anastasiou, A.; Dimitropoulos, N.; Kalivas, N.; Ventouras, E.; Kalatzis, I.; Nomicos, C.; Panayiotakis, G. Evaluation of ZnS:Cu phosphor as X-ray to light converter under mammographic conditions. *Radiat. Meas.* **2005**, *39*, 263–275. [[CrossRef](#)]
29. Cavouras, D.; Kandarakis, I.; Nikolopoulos, D.; Kalatzis, I.; Kagadis, G.; Kalivas, N.; Episkopakis, A.; Linardatos, D.; Roussou, M.; Nirgianaki, E.; et al. Light emission efficiency and imaging performance of Y₃Al₅O₁₂:Ce (YAG:Ce) powder screens under diagnostic radiology conditions. *Appl. Phys. B* **2005**, *80*, 923–933. [[CrossRef](#)]
30. Seferis, I.E.; Zeler, J.; Michail, C.; Valais, I.; Fountos, G.; Kalyvas, N.; Bakas, A.; Kandarakis, I.; Zych, E. On the response of semitransparent nanoparticulated films of LuPO₄:Eu in poly-energetic X-ray imaging applications. *Appl. Phys. A* **2016**, *122*. [[CrossRef](#)]
31. Michail, C.; Kalyvas, N.; Bakas, A.; Ninos, K.; Sianoudis, I.; Fountos, G.; Kandarakis, I.; Panayiotakis, G.; Valais, I. Absolute Luminescence Efficiency of Europium-Doped Calcium Fluoride (CaF₂:Eu) Single Crystals under X-ray Excitation. *Crystals* **2019**, *9*, 234. [[CrossRef](#)]
32. Nikolopoulos, D.; Kalyvas, N.; Valais, I.; Argyriou, X.; Vlamakis, E.; Sevvos, T.; Kandarakis, I. A semi-empirical Monte Carlo based model of the Detector Optical Gain of Nuclear Imaging scintillators. *J. Instrum.* **2012**, *7*, P11021. [[CrossRef](#)]
33. Kalyvas, N.; Valais, I.; David, S.; Michail, C.; Fountos, G.; Liaparinos, P.; Kandarakis, I. Studying the energy dependence of intrinsic conversion efficiency of single crystal scintillators under X-ray excitation. *Opt. Spectr.* **2014**, *116*, 743–747. [[CrossRef](#)]
34. Kalyvas, N.; Valais, I.; Michail, C.; Fountos, G.; Kandarakis, I.; Cavouras, D. A theoretical study of CsI:Tl columnar scintillator image quality parameters by analytical modeling. *Nucl. Instrum. Methods Phys. Res.* **2015**, *779*, 18–24. [[CrossRef](#)]
35. David, S.; Michail, C.; Seferis, I.; Valais, I.; Fountos, G.; Liaparinos, P.; Kandarakis, I.; Kalyvas, N. Evaluation of Gd₂O₂S:Pr granular phosphor properties for X-ray mammography imaging. *J. Lumin.* **2016**, *169*, 706–710. [[CrossRef](#)]
36. Kalivas, N.; Costaridou, L.; Kandarakis, I.; Cavouras, D.; Nomicos, C.D.; Panayiotakis, G. Effect of intrinsic-gain fluctuations on quantum noise of phosphor materials used in medical X-ray imaging. *Appl. Phys. A Mater. Sci. Process.* **1999**, *69*, 337–341. [[CrossRef](#)]
37. Zhang, F.; He, X.; Ma, P.; Sun, Y.; Wang, X.; Song, D. Rapid aqueous synthesis of CuInS/ZnS quantum dots as sensor probe for alkaline phosphatase detection and targeted imaging in cancer cells. *Talanta* **2018**, *189*, 411–417. [[CrossRef](#)]

38. Shakur, H.R. A detailed study of physical properties of ZnS quantum dots synthesized by reverse micelle method. *Physica. E Low Dimen Syst. Nanostruct.* **2011**, *44*, 641–646. [[CrossRef](#)]
39. Mathew, S.; Bhardwaj, B.S.; Saran, A.D.; Radhakrishnan, P.; Nampoore, V.P.N.; Vallabhan, C.P.G.; Bellare, J.R. Effect of ZnS shell on optical properties of CdSe–ZnS core–shell quantum dots. *Opt. Mater.* **2015**, *39*, 46–51. [[CrossRef](#)]
40. Fiaczyk, K.; Zych, E. On peculiarities of Eu^{3+} and Eu^{2+} luminescence in Sr_2GeO_4 host. *RSC Adv.* **2016**, *6*, 91836–91845. [[CrossRef](#)]
41. Zeler, J.; Cybińska, J.; Zych, E. A new photoluminescent feature in $\text{LuPO}_4:\text{Eu}$ thermoluminescent sintered materials. *RSC Adv.* **2016**, *6*, 57920–57928. [[CrossRef](#)]
42. Jacobsohn, L.G.; Bennett, B.L.; Muenchausen, R.E.; Smith, J.F.; Wayne Cooke, D. Luminescent properties of nanophosphors. *Radiat. Meas.* **2007**, *42*, 675–678. [[CrossRef](#)]
43. Refractiveindex.info. Available online: <https://refractiveindex.info> (accessed on 3 July 2019).
44. Nowotny, R. XMuDat: Photon attenuation data on PC. *International Atomic Energy Agency, Nuclear Data Section*. Available online: <https://www-nds.iaea.org/publications/iaea-nds/iaea-nds-0195.htm> (accessed on 3 July 2019).
45. Plasmachem. Available online: www.plasmachem.com/shop/en/278-530-15-nm (accessed on 3 July 2019).
46. Saatsakis, G.; Michail, C.; Fountzoula, C.; Kalyvas, N.; Bakas, A.; Ninos, K.; Fountos, G.; Sianoudis, I.; Kandarakis, I.; Panayiotakis, G.S.; et al. Fabrication and Luminescent Properties of Zn–Cu–In–S/ZnS Quantum Dot Films under UV Excitation. *Appl. Sci.* **2019**, *9*, 2367. [[CrossRef](#)]



© 2019 by the authors. Licensee MDPI, Basel, Switzerland. This article is an open access article distributed under the terms and conditions of the Creative Commons Attribution (CC BY) license (<http://creativecommons.org/licenses/by/4.0/>).